Philosophical Magazine
Vol. 91, Nos. 7–9, 1–21 March 2011, 1339–1355

Taylor & Francis
Taylor & Francis Group

Dynamic impact indentation of hydrated biological tissues and tissue surrogate gels

Z. Ilke Kalcioglu[a], Meng Qu[a], Kenneth E. Strawhecker[b], Tarek Shazly[c], Elazer Edelman[c], Mark R. VanLandingham[b], James F. Smith[d] and Krystyn J. Van Vliet[a]*

[a]*Department of Materials Science and Engineering, Massachusetts Institute of Technology, Cambridge, MA 02139, USA;* [b]*US Army Research Laboratory, 4600 Deer Creek Loop, Aberdeen Proving Ground, MD 21005, USA;* [c]*Harvard-MIT Division of Health Sciences and Technology, Massachusetts Institute of Technology, Cambridge, MA 02139, USA;* [d]*Micro Materials, Ltd., Wrexham, UK*

(*Received 10 December 2009; final version received 27 July 2010*)

For both materials engineering research and applied biomedicine, a growing need exists to quantify mechanical behaviour of tissues under defined hydration and loading conditions. In particular, characterisation under dynamic contact-loading conditions can enable quantitative predictions of deformation due to high rate 'impact' events typical of industrial accidents and ballistic insults. The impact indentation responses were examined of both hydrated tissues and candidate tissue surrogate materials. The goals of this work were to determine the mechanical response of fully hydrated soft tissues under defined dynamic loading conditions, and to identify design principles by which synthetic, air-stable polymers could mimic those responses. Soft tissues from two organs (liver and heart), a commercially available tissue surrogate gel (Perma-Gel^{TM}) and three styrenic block copolymer gels were investigated. Impact indentation enabled quantification of resistance to penetration and energy dissipative constants under the rates and energy densities of interest for tissue surrogate applications. These analyses indicated that the energy dissipation capacity under dynamic impact increased with increasing diblock concentration in the styrenic gels. Under the impact rates employed (2 mm/s to 20 mm/s, corresponding to approximate strain energy densities from 0.4 kJ/m^3 to 20 kJ/m^3), the energy dissipation capacities of fully hydrated soft tissues were ultimately well matched by a 50/50 triblock/diblock composition that is stable in ambient environments. More generally, the methodologies detailed here facilitate further optimisation of impact energy dissipation capacity of polymer-based tissue surrogate materials, either in air or in fluids.

Keywords: tissue surrogate; impact indentation; energy dissipation; liver; heart

*Corresponding author. Email: krystyn@mit.edu.

ISSN 1478–6435 print/ISSN 1478–6443 online

DOI: 10.1080/14786435.2010.512574
http://www.informaworld.com

1. Introduction

There exists a growing need to quantify the mechanical behaviour of tissues under dynamic loading conditions. Such studies enable prediction of the deformation and energetic dissipation under high-rate loading 'impact events' such as industrial accidents, ballistic injuries and blasts [1,2]. In addition, there exists a concurrent need for tissue surrogate materials, synthetic materials capable of simulating the mechanical responses of biological tissues. Tissue surrogates serve as mechanical mimics of hydrated tissues, and can be examined in ambient conditions under controlled laboratory testing. These materials are used to help evaluate tissue-engineering designs and the efficacy of technologies including protective garments [3]. Thus, tissue surrogates must be synthesised reproducibly, and must enable application of repeated, defined loading conditions that are similar to the forces applied to the fully hydrated soft tissues they are intended to mimic mechanically.

A growing number of reports have quantified mechanical properties of soft tissues via a variety of quasistatic methods including macroscale tension, unconfined compression and microscale indentation experiments [4–11]. Further, dynamic mechanical analysis of soft tissues have been explored via methods such as oscillatory loading [12–15] and indentation recovery [16]. However, the mechanical response of soft tissues to impact loading at the high rates relevant to insult and injury is relatively less explored. Recent macroscopic studies have included falling-weight impact tests [17], Kolksy or split Hopkinson pressure bar-based experiments [2,18–20], instrumented impacters [21] and blunt impact tests using a pendulum-like apparatus [22,23]. These macroscale approaches are certainly important as a first step in characterising responses of soft tissues under impact loading, and can facilitate comparisons among tissue types. However, most such studies to date have explored the energy dissipation capacity of tissues in ambient air rather than fully hydrated environments that define the relevant structure and mechanical properties of biological tissues [24]. This shortfall motivates the design of new techniques that enable measurement of multiscale mechanical properties of hydrated tissues, under extreme loading conditions. Such methods could also aid in the development of highly compliant synthetic materials for a variety of biomedical and other applications.

Here, we demonstrate that contact loading via impact indentation can be employed to characterise the mechanical behaviour of hydrated tissues and tissue surrogate materials under concentrated impact. We first adapt the experimental methods and analysis, initially proposed for metals and glassy polymers [25,26], to address key differences in the application to soft tissues in hydrated environments. We then demonstrate the application of this approach to characterising the impact energy dissipation and resistance to penetration of tissues and tissue surrogate gels that are intended to replicate the tissue responses under impact loading conditions. Such analysis enables identification of design principles by which tissue surrogate materials can be engineered to better match the dynamic response of specific soft tissues under comparable mechanical deformation states, rates, and insults. More specifically, we employed microscale contact-loading methods to quantify the mechanical response of mammalian liver and heart tissues. These tissues are located in the abdominal and chest cavities, respectively, and are commonly damaged by

high-impact mechanical insults. We compared a commercially available tissue surrogate, Perma-Gel^{TM}, with blends of styrenic triblock (ABA) and diblock (AB) copolymers [1]. Dynamic impact loading indicated the opportunity to tune the energy dissipation of the block copolymers as a function of diblock content. Under the impact conditions of interest, we were thus able to identify design principles and triblock/diblock compositions that best matched the impact resistance and energy dissipation of hydrated heart and liver tissues.

2. Experimental methods and analyses

2.1. *Materials and tissues*

Two types of synthetic materials were considered as potential surrogates of tissue impact response, including Perma-Gel^{TM} (Perma-Gel, Inc.), a commercial ballistic organogel of proprietary composition that is physically stable at room temperature [27]; and gels formed from styrenic block copolymers (Kraton Polymers) comprised of styrene (S) and either ethylene/butylene (EB) or ethylene/propylene (EP). Copolymer-based gel samples were made by mixing SEBS triblock copolymer (Kraton G1652) with SEP diblock copolymer (Kraton G1701). The copolymers were dissolved at elevated temperature in light mineral oil (Mallinckrodt Chemicals, St. Louis, MO) at a volume ratio of 20:80 polymer to oil, forming gels upon cooling to room temperature. Each polymer–oil mixture was placed in a vacuum oven at 150°C and fully dissolved over 6 h with stirring every hour. The melt was then poured onto a flat surface to cool and gelate. Light mineral oil is a block selective solvent, i.e. a good solvent for the rubbery blocks and a poor solvent for the styrene blocks, and has a low vapour pressure facilitating development of physically associating gels that are stable in ambient conditions. Samples were mixed at triblock:diblock volume ratios of 100/0, 75/25 and 50/50, and cast to obtain final sample thickness of 4 mm. Note that both types of gels were stable under ambient conditions of laboratory air humidity and temperature, and are intended to be used in ambient air for tissue surrogate applications. Thus, our structural and mechanical characterisation of these gels was carried out in ambient air.

Tissues were harvested from healthy male, adult Sprague-Dawley rats (250–350 g). All experiments involving animals were approved by the university IACUC protocol and compliant with NIH guidelines for animal care. The structure and mechanical behaviour of these tissues depends strongly on hydration state [24], and change with cell lysis and protein degradation *ex vivo*. The goal of this study was to identify and replicate the mechanical response of these tissues to concentrated impact in near-physiological conditions. Thus, all experiments were conducted within 3 h post mortem. For both heart and liver tissue, discs of 8 mm diameter and thickness of 3 to 5 mm were prepared using a surgical punch, and all tissues were stored in Krebs–Henseleit buffer immediately after excision and throughout all experiments reported herein.

Soft tissues exhibit a striated or orthotropic anisotropy at the microscale dimensions relevant to indentation-based experiments considered herein, whereas the synthetic gels are structurally homogeneous at the microscale (Figures 1a–c). Approaching the nanoscale, however, structural anisotropy in the synthetic gels

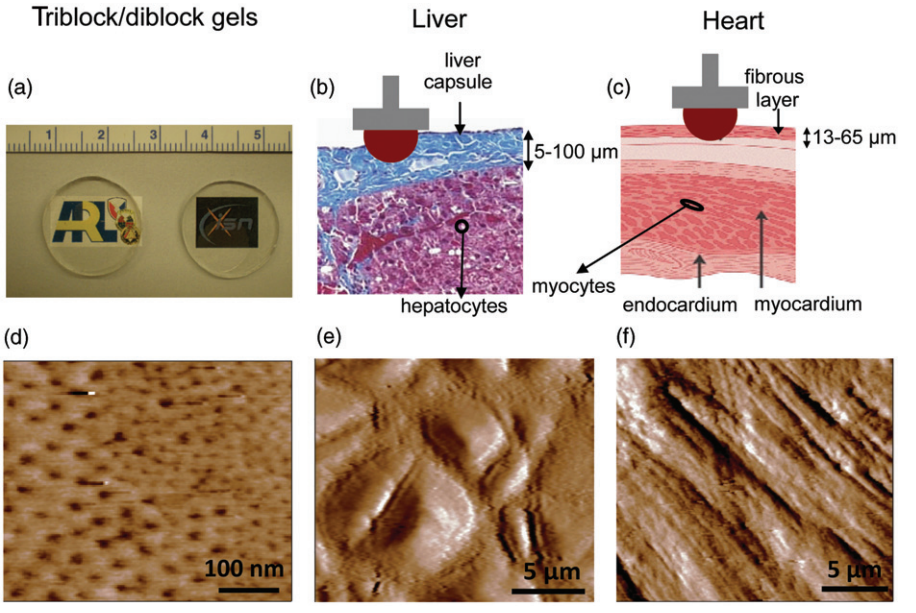

Figure 1. (a) 100/0 and 75/25 triblock/diblock styrenic copolymer discs of diameter ~2 cm. (b) Schematic illustrating length scales of liver tissue structural heterogeneity (adapted from [28] with permission from R.A. Bowen) with respect to indenter probe diameter and contact depths in these experiments, for which penetration proceeded normal to the outer liver capsule. (c) Schematic illustrating length scales of heart tissue structural heterogeneity (adapted from [29] with permission from Remedica Medical Education and Publishing) with respect to indenter probe diameter and contact depths in these experiments, for which penetration proceeded normal to the outer fibrous layer. AFM phase-lag image of (d) 75/25 triblock/diblock styrenic copolymer, indicating segregated domains of triblocks and diblock–triblocks, (e) rat liver capsule and (f) fibrous layer of rat heart.

becomes apparent in terms of micelle formation (Figure 1d). The difference in structures of these materials is observable in atomic force microscopy (AFM) phase contrast images, as shown in Figures 1d–f. These images were acquired using a 3D MFP AFM (Asylum Research) in AC mode at a scan rate of 0.5 Hz; images were acquired in ambient air for synthetic organogels and in Krebs–Henseleit buffer for tissues.

As schematised in Figure 2, AB (SEP) diblock chains contain the A block within the micellar core and the B block extending away from the micelle into the solution (i.e. adding no network connectivity). In contrast, the ABA (SEBS) triblock chains can form either loops when both A blocks are in the same micelle; chains when only one A block is in a micelle with the rest of the triblock extending into solution; or bridges when A blocks are in neighbouring micelles connected by the B block [30]. Thus, the microstructure of these synthetic gels can be manipulated by tuning the relative concentration of triblock to diblock, in that increasing the vol. %-triblock will result in a higher crosslinking density of the gel. Whereas the apparent diameters of the micelles in Figure 1d are slightly enlarged by the finite AFM probe size and probe–sample contact, these features are considerably smaller than the μm-scale

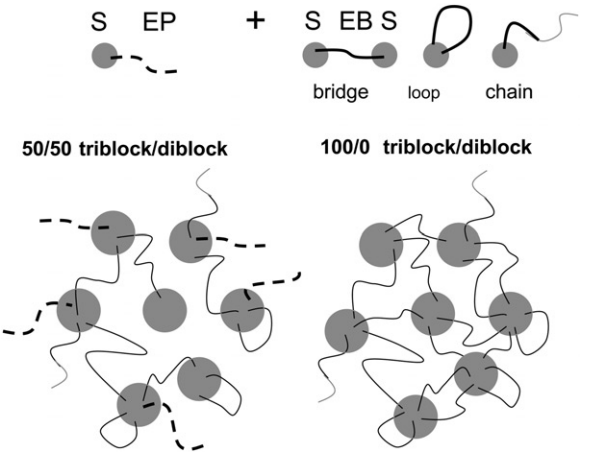

Figure 2. Styrenic block copolymers comprise AB diblocks of styrene–ethylene propylene (SEP), and ABA triblocks of styrene–ethylene butylene (SEBS). As the vol. %-triblock increases, crosslinking density of the gel will increase, since in ABA (SEBS) triblocks, B blocks can form bridges between different micellar cores containing the A blocks (adapted from [31]).

structures such as cuboidal and elongated cells of the hepatic lobules and cardiac muscle tissue of liver and heart, respectively (Figures 1e–f).

2.2. *High-rate impact indentation experiments*

For both gels and tissues, impact experiments were conducted to ascertain the dynamic response of materials under concentrated impact loading at elevated rates. Pendulum-based impact experiments were conducted using a commercial instrumented indenter (Micro Materials, Ltd.) as described previously [25,26], using a stainless steel probe of radius $R = 2\,\text{mm}$ on all materials. Gels adhered readily and strongly to a bulk aluminium alloy support. Tissues were adhered to the aluminium support with a thin layer of cyanoacrylate ($< 5\,\mu\text{m}$, as compared to the 3 to 5 mm scale thickness of these tissues). Tissue samples were fully immersed in Krebs–Henseleit buffer using the modified platform for fluid immersed experiments we have described previously [32]. The force pendulum in this instrument is actuated to apply load via electromagnetic interaction between the conductive coil at its 'top' toward the stationary magnetic plate positioned behind the coil, and articulates about a frictionless pivot of compliant leaf springs; displacement of the probe mounted rigidly toward the 'bottom' of the pendulum is measured via a parallel-plate capacitor. To achieve impact loading, the pendulum position is maintained via a solenoid/magnet assembly below the probe, while the electromagnetic coil current above the probe is increased; shutting off the solenoid then releases the 'loaded' pendulum such that the probe swings toward the sample with high kinetic energy. Resulting probe displacement is recorded as a function of time, until the probe comes to rest at the sample surface. Here, the physical limit stop (which sits behind the

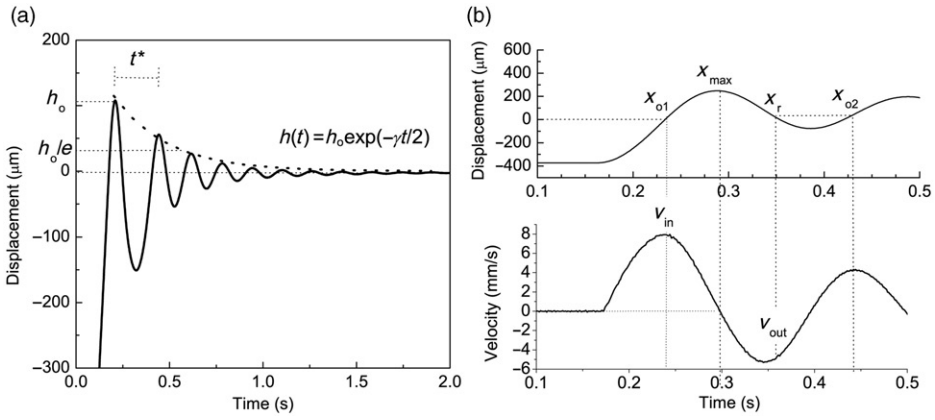

Figure 3. Representative impact response and definition of terms used to quantify energy dissipation. (a) Pendulum displacement over time is described by damped harmonic oscillatory motion, here for a 100/0 triblock/diblock gel at an impact velocity of 5.8 mm/s. Quality factor Q is calculated via Equation (2), and can be recognised visually as the number of indentation impact cycles n required for the amplitude of oscillation h_o to fall by a factor of e. Here, $n \sim 2$ so $Q \sim 6$. (b) Velocity is calculated as the time derivative of displacement. Impact velocity v_{in} is the maximum velocity prior to contact, which defines the sample contact point x_{o1}. To objectively identify the position of the deformed surface, x_r is taken to be equivalent to the displacement x_{o2}, which would be required to initiate contact with the sample in the next cycle. Thus x_r is the position of the relaxed surface following the initial impact. Rebound velocity v_{out} is defined as the velocity at displacement x_r. Penetration depth over the first impact cycle is defined as $x_{\max} - x_{o1}$.

pendulum for quasistatic indentation experiments) was retracted to achieve both high impact velocities and high impact penetration depths into such compliant samples to remove this potential obstruction of the pendulum motion. Impact velocities investigated here ranged from 2 to 20 mm/s. For the probe of mm-scale radius employed in the present experiments, the resulting strain energy density depends naturally on each material's resistance to penetration, and ranged from 0.4 to 20 kJ/m^3 among all samples.

2.3. *Analysis of energy dissipation from impact indentation experiments*

In general, pendulum based impact tests conducted here can be fully described by damped harmonic oscillatory motion (Figure 3a). This response upon impact and subsequent oscillation against the sample is well fit by an exponentially decaying time-dependent function of the indenter displacement, upon impact and oscillation against a sample [33]:

$$h(t) = h_o \exp(-\gamma t/2), \tag{1}$$

where $\gamma/2$ is the inverse of the decay time τ of the pendulum oscillation. Natural angular frequency ω is measured by $\omega = 2\pi/t^*$, where t^* is the measured period of oscillation.

Energy dissipation upon impacting the sample can be calculated as the effective quality factor Q of the damped oscillatory system. This Q is a dimensionless number that we here compute as

$$Q = \frac{\omega}{\gamma} = \frac{2\pi}{\gamma t^*} \tag{2}$$

for a measured $h(t)$ response. Equivalently, $Q/2\pi$ is the ratio of energy stored per cycle to energy lost per cycle [34]. For completeness, we note that qualitative differences in Q can be observed directly from the $h(t)$ response: the number of indentation impact cycles n required for the amplitude of oscillation to fall by a factor of e occurs over approximately Q/π cycles of oscillation (see Figure 3a) [33].

Energy dissipation upon impact can also be determined directly from analysis of the first impact cycle, rather than from the decay of oscillation that is used to determine Q, as the ratio of impact and rebound velocities (see Figure 3b). For each impact experiment, the following parameters were calculated from customised analysis scripts in MATLAB (The MathWorks, Inc.): impact (v_{in}) and rebound (v_{out}) velocities, displacement at which contact initiates (x_{o1}) displacement at maximum penetration ($x_{\max}$) and displacement at minimum rebound velocity (x_r). Impact energy E_{imp} was calculated from $E_{\text{imp}} = (\frac{1}{2})mv_{\text{in}}^2$, and strain energy densities were calculated as impact energy normalised by the geometric contact volume of the spherical probe at $x_{\max}$.

Here, v_{out} is used to calculate the elastic energy that is recovered during the unloading portion of the first impact. If v_{out} corresponded exactly to the exit velocity upon loss of contact and if the energy dissipation mechanisms were solely due to inelastic deformation and local heating, $v_{\text{out}}/v_{\text{in}}$ would be termed the coefficient of restitution. In the gels and tissues studied herein, adhesion forces serve as an additional source of energy dissipation. We observed visually that the probe tended to remain in contact with the surface upon rebound; this is attributable to high adhesive forces between the probe and the sample, even under the fully hydrated and buffered conditions of these tissues. Therefore, we characterise these more complex collisions simply as $v_{\text{out}}/v_{\text{in}}$. This ratio was compared among materials at a given impact velocity and among impact velocities for a given material.

Both Q and $v_{\text{out}}/v_{\text{in}}$ quantify the energy dissipation of the sample–pendulum system. To distinguish the energy dissipation capacity of the sample alone, which we will define as the dimensionless parameter K, we must first calculate the energy dissipated and recovered by the pendulum as outlined below in Equations (3)–(7). In general, at any given displacement of the pendulum after impact is initiated, the impact energy is the total energy of the system (pendulum and sample) and can be defined as

$$E_t^{\text{system}} = \left(\frac{1}{2}\right)m(v_{\text{in}})^2 = E_r^s + E_r^p + E_d^s + E_d^p, \tag{3}$$

where E_r^s is the energy recovered by the sample, E_r^p is the energy restored to the system by the fully recovered displacement of the pendulum springs at v_{out}, E_d^s is the energy dissipated by the sample, and E_d^p is the energy dissipated by the pendulum. The latter dissipation can be attributed to sources such as Eddy current damping at

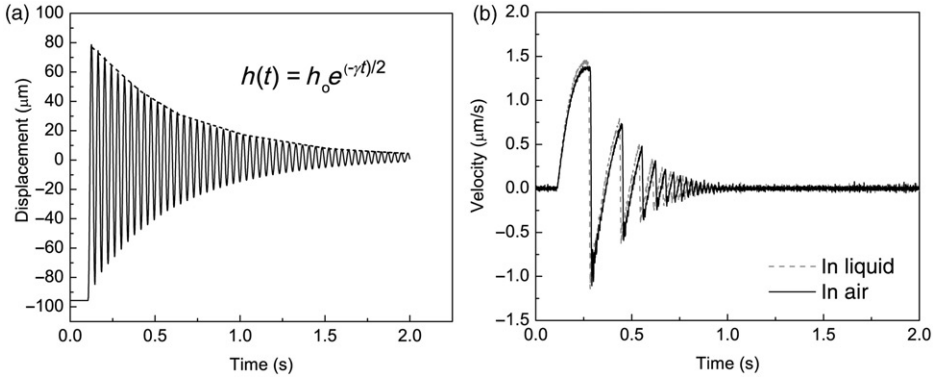

Figure 4. (a) Free oscillations of the pendulum–linear elastic wire spring system show that the damping due to the pendulum is small but not negligible. Pendulum damping constant b_p is calculated via Equation (6), ω_o and γ_m are extracted by fitting Equation (1) to the $h(t)$ response. (b) Differences in pendulum velocity for oscillations in air or immersed in fluid do not differ significantly, showing that immersion in aqueous environments contributes negligible additional damping.

the electromagnetic coil/magnet, air damping between the capacitor plates, etc. Note that the subscripts r and d indicate restored and dissipated energies, respectively; superscripts s and p denote the sample and pendulum, respectively. Total recovered energy at v_{out} is calculated from

$$\left(\frac{1}{2}\right)m(v_{\text{out}})^2 = E_r^s + E_r^p. \tag{4}$$

Therefore, to calculate accurately the energy dissipated only by the sample at v_{out}, we require calculation of E_d^p and E_r^p at v_{out}. The restored energy of the pendulum E_r^p is calculated from the relation

$$E_r^p = \left(\frac{1}{2}\right)k_p(\Delta x)^2, \tag{5}$$

where $\Delta x = x_{\max} - x_r$, which is the distance the pendulum travels out of the impacted sample from its maximum penetration depth during the unloading portion of this impact, and k_p is the effective rotational stiffness of the pendulum at the indenter contact position.

To calculate the dissipated energy of the pendulum E_d^p the dynamic response of the pendulum must also be calibrated as we have detailed previously [26]. Briefly, we determined the pendulum damping coefficient b_p (0.6 N s/m) and pendulum quality factor Q_p (46.1) via analysis of $h(t)$ for abrupt loading experiments on a wire spring connected between the pendulum and opposing sample holder (Figure 4a). In order to provide analysis of multiple oscillations in a relatively short test period, the stiffness of this spring was chosen to be much higher ($k_{\text{spring}} = 4.457$ kN/m) than the low rotational stiffness of the pendulum ($k_p = 3$ N/m). This rotational stiffness was measured from the slope of force–displacement response prior to physical contact

between the probe and the surface under quasistatic rates. The pendulum damping coefficient is calculated as

$$b_p = \frac{\gamma_m k_{\text{spring}}}{\omega_0^2}, \tag{6}$$

where γ_m ($3.5\,\text{s}^{-1}$) was determined from fitting Equation (1) to the $h(t)$ response of Figure 4a and the angular resonant frequency of the pendulum–wire spring system ω_o ($161.6\,\text{rad}\,\text{s}^{-1}$) was determined directly from this same $h(t)$ response. The magnitude of Q_p was determined as ω_o/γ_m. No significant damping due to the presence of liquid was observed (Figure 4b). Therefore, the energy dissipation and system damping analysis outlined here hold for experiments on both gels tested in air and tissues tested in aqueous Krebs–Henseleit buffer. Finally, the dissipated energy of the pendulum E_d^p is then calculated as

$$E_d^p = \int_{x_o}^{x_{\max}} b_p \frac{\partial x}{\partial t}\,\mathrm{d}x + \int_{x_{\max}}^{x_r} b_p \frac{\partial x}{\partial t}\,\mathrm{d}x. \tag{7}$$

Having calibrated pendulum energy dissipation, we can now consider the energy dissipated only by the sample under impact. Using Equations (3)–(5) and (7), we can calculate the quantity K, which is the energy dissipated by the sample normalised to the sum of the dissipated and recovered sample energy:

$$K = \frac{E_d^s}{E_t^{\text{system}} - E_r^p - E_d^p}. \tag{8}$$

In summary, impact analysis provides three quantitative measures of energy dissipation: Q (Equation (2)), $v_{\text{out}}/v_{\text{in}}$, and K (Equation (8)). Note that whereas $v_{\text{out}}/v_{\text{in}}$ and K characterise the magnitude or extent of energy dissipation by the material during the first impact cycle, Q indicates the rate of energy dissipation.

3. Results and discussion

Impact indentation experiments were conducted on Perma-Gel$^{\text{TM}}$, styrenic block copolymer gels, and liver and heart tissues at impact velocities up to 20 mm/s. Figure 5 shows representative impact responses of tissues and gels for an impact velocity of 7 mm/s and corresponding impact energy of 4 μJ. These raw displacements vs. time responses enable one to readily compare both the deformation response and the rate of energy dissipation among samples qualitatively. First, these data indicated that the hydrated tissues were more compliant than these gels, as the tissues exhibit the maximum deformation (i.e. depth of penetration) under a given impact velocity and impact energy. Among the styrenic block copolymers, Figure 5 clearly shows that the maximum penetration depth, $x_{\max}$, increased with decreasing vol. %-triblock. Perma-Gel$^{\text{TM}}$ exhibited an intermediate deformation between that of the 75/25 and 50/50 triblock/diblock gels. Second, Figure 5 illustrates the rate of energy dissipation among samples in terms of the number of indentation impact cycles to dissipate the total impact energy, as apparent from the number and duration of pendulum oscillations after impact. Whereas Perma-Gel$^{\text{TM}}$ and 100/0

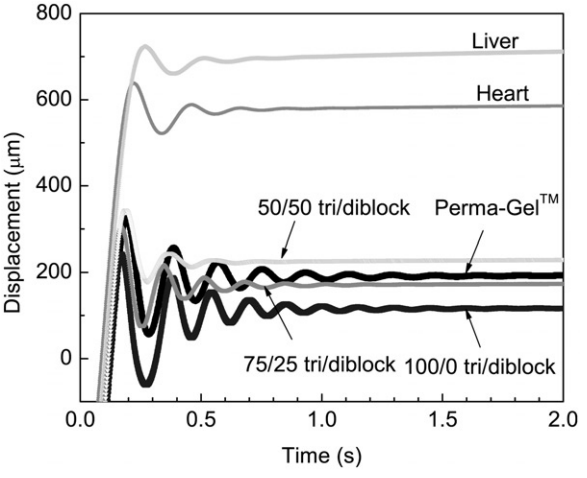

Figure 5. Impact loading was conducted using a customised, pendulum-based nanoindenter. Raw displacement vs. time response for all materials at a maximum velocity of 7 mm/s corresponding to impact energy of 4 μJ shows a significant difference between the penetration depths and energy dissipation rates among all samples.

triblock/diblock gel dissipated impact energy most slowly, the tissues dissipated impact energy most quickly. Among the triblock/diblock styrenic gels, the number of cycles and time for complete energy dissipation increases with increasing vol. %-triblock. In fact, Figure 5 shows that 50/50 triblock/diblock dissipated total impact energy almost as quickly as the tissues for this impact velocity. This qualitative comparison among impact displacement responses indicates that the rate of impact energy dissipation can be tuned towards that of heart and liver tissues by modulating the triblock concentration. Next, we quantitatively evaluate the impact responses in terms of penetration depth and energy dissipation capacity, under a range of impact velocities and strain energy densities.

3.1. *Penetration resistance under dynamic impact loading*

To compare the penetration resistance of each sample quantitatively, displacement of the pendulum at maximum penetration, x_{max}, is calculated as a function of impact velocity. For the range of impact energies studied here, the resistance of a material to impact penetration decreases with increasing impact velocity (Figure 6a); however, the trends of maximum penetration among the different materials as described above still hold. Here, the maximum impact velocities obtained for tissues were lower than that attained for gels. For the compliant hydrated tissues, an impact velocity $v_{in} > 8$ mm/s imposed via this probe would penetrate the tissue so deeply that the pendulum displacement would be physically halted due to mechanical collision of the electromagnetic coil into the stationary magnetic plate. Higher impact velocities on tissues could be attained via probes of larger radii, but with concurrent and nonlinear decreases in impact energy densities due to the high compliance of these tissues.

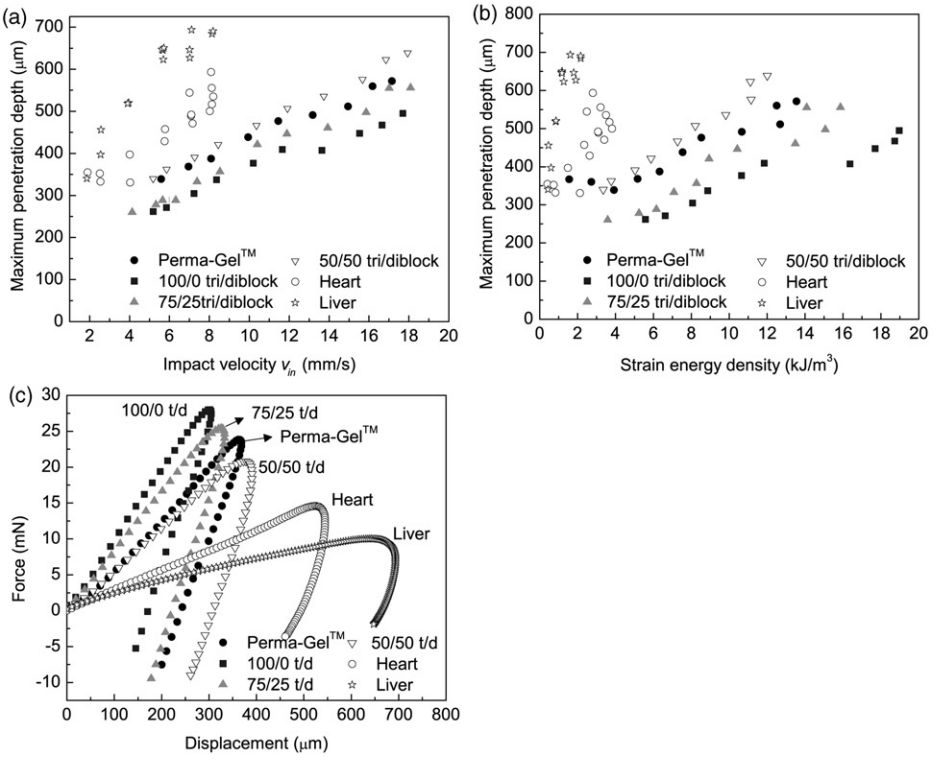

Figure 6. Maximum penetration depths varied as a function of (a) impact velocity and (b) strain energy density. Liver tissue exhibited the lowest penetration resistance among all samples whereas 50/50 triblock/diblock gel exhibited the closest penetration resistance to heart tissue. (c) Force–displacement responses calculated from the $h(t)$ response of the first impact peak for an impact energy of ~4 μJ show significant hysteresis for all samples. As observed in (a) and (b), liver tissue exhibited the lowest penetration resistance.

As expected, maximum penetration depth also varied with imposed strain energy density (Figure 6b). Although the velocities investigated here are still low compared to ballistic tests (mm/s compared to ~m/s), the impact strain energy densities are high (0.4–20 kJ/m^3) and comparable with macroscale impact tests such as pneumatic gun and falling weight impacts designed to replicate ballistic conditions (15–60 kJ/m^3 [17]). The high strain energy density achievable in the present contact-based impact experiments is due simply to the fact that the contact volumes of impact indentation are over contact areas on the order of hundreds of μm^2, as compared to contact areas on the order of cm^2 for macroscopic ballistic impact. Note that our reported impact energy densities represent an upper bound, as these are calculated from penetration depth and thus neglect the actual volume of material under significant strain beneath the impact contact. Actual contact areas and strain volumes will depend on whether the material is structurally homogeneous over the experiment length scales or exhibits structural heterogeneity. The lamellar structure of encapsulated and striated tissues imposes such uncertainties in strain energy density calculations.

Finally, the displacement vs. time response at the first impact peak can also be represented as a force vs. displacement response that allows visualisation of hysteresis curves for a given impact velocity. For alternative probe geometries such as flat punch, this response can further be transformed to stress vs. strain, which is a metric that is reported by other macroscale pendulum-based impact approaches and split-Hopkinson pressure bar experiments [2,22]. The resistive force of the material is defined as $F = ma$, where a is the deceleration of the pendulum upon impact and m is the mass of the pendulum (impacting object). This calculated force changes as a function of penetration and rebound depths (Figure 6c). Under similar impact energies, all samples exhibited significant hysteresis. The 100/0 triblock/diblock gel showed the stiffest response, and these gels were increasingly compliant with decreasing vol. %-triblock. This trend is expected from the higher crosslinking concentration of the triblock phase [1,35]: the replacement of SEBS chains by SEP chains induces a decrease in the number of bridges that can act as physical crosslinks between micelles. In contrast, liver tissue exhibited the most compliant response among all samples. The comparative compliance of liver tissue as compared to heart tissue at these elevated deformation rates is consistent with quasistatic mechanical comparisons of elastic moduli, E, between two tissue types, estimated via macroscale uniaxial compression, uniaxial tension, and indentation experiments [6,7,36,37].

Note that Figure 6c also underscores the difference in penetration depth between the gels and these tissues. If the goal of the tissue surrogate gel is to dissipate the total impact energy at penetration depths comparable to these tissues, none of the gels considered here are viable candidates. The tunability of decreased penetration depth with increasing vol. %-triblock is apparent in Figures 6a–c, but further decreases in vol. %-triblock are not possible for this particular system due to incomplete gelation for <50 vol. %-triblock compositions. However, the bridging role of the triblocks in impact penetration resistance of such block copolymers provides a clear avenue for development of other tissue surrogate gels. Next, we compare the rate and extent of impact energy dissipation among these gels and tissues.

3.2. *Energy dissipation under dynamic impact loading*

To compare the energy dissipation capacity of each pendulum-sample system quantitatively, two dimensionless parameters were considered. First, the velocity ratio $v_{out}/v_{in,}$ which provides a measure of the material energy dissipation per impact; this reduction in velocity upon impact considers only the first instance of reversible penetration between the indenter probe and material, such that energy dissipated by the dynamic indentation event modulates v_{out}/v_{in}. Second, the quality factor Q as defined in Equation (2) provides a measure of the rate of energy dissipation in the pendulum-sample system, determined over multiple impact events until complete dissipation of the impact energy.

Figures 7a and b show average v_{out}/v_{in} and Q, respectively, for the tissues and tissue surrogate gels under the impact velocities considered herein. Both measures of energy dissipation indicate that tissues exhibit a higher impact energy dissipation capacity than the tissue surrogate gels, at least over the velocities and impact energy densities of interest. That is, more energy is dissipated in a single impact cycle

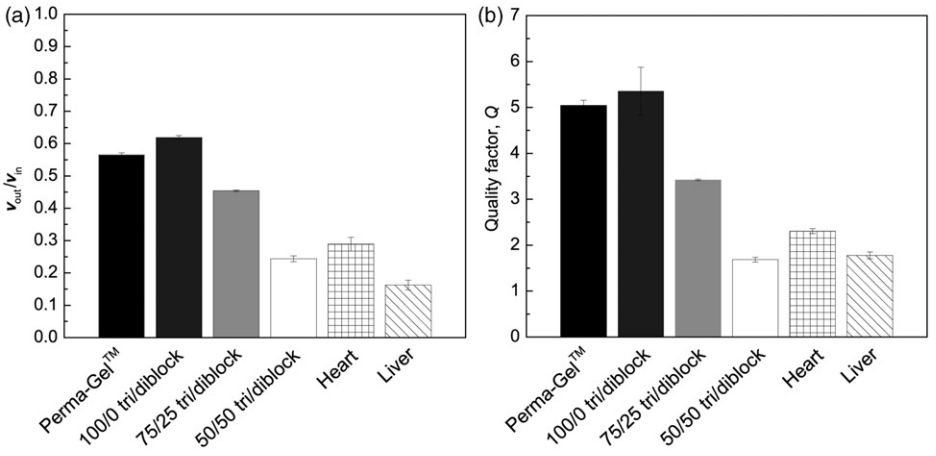

Figure 7. (a) Velocity ratio v_{out}/v_{in} and (b) quality factor Q for the impact energies studied here provide means to compare the energy dissipation capacity and energy dissipation rate of each sample, averaged over the range of impact velocities considered. Comparison of v_{out}/v_{in} shows that Perma-Gel™ and 100/0 triblock/diblock gel exhibit the lowest energy dissipation capacity, whereas energy dissipation capacity of 50/50 triblock/diblock gel is similar to that of liver and heart tissues. Comparison of Q shows that both Perma-Gel™ and 100/0 triblock/diblock gel dissipate the total energy more slowly, as compared to 50/50 triblock/diblock gel and tissues. Data indicated as mean ± standard error.

(v_{out}/v_{in}) and total impact energy is dissipated more quickly (Q) in these tissues. Note that the quality factor of the pendulum-based indenter is at least one order of magnitude higher than those observed on the more dissipative tissues and tissue surrogate gels. This is expected since Q of a system is large compared to unity for impact of materials and/or conditions exhibiting small rates of energy dissipation (i.e. more cycles of oscillation to achieve a given decrease in the depth of penetration or amplitude of oscillation). Conversely, a system of low Q is a 'lossy' one, such that a larger fraction of the imposed impact energy will be dissipated over the first cycle, and the total impact energy will be fully dissipated over a shorter duration of time.

Perma-Gel™ and 100/0 triblock/diblock gel exhibited the lowest impact energy dissipation capacity among these materials, and liver tissue exhibited the greatest impact energy dissipation capacity. Although Perma-Gel™ is more compliant than the 75/25 triblock/diblock gels (i.e. the maximum depth of penetration is larger at all impact velocities considered in Figure 6a), the dissipation capacity of this ballistic gel is less than that of the styrenic gel comprising 75 vol. %-triblock. This result likely reflects differences in the proprietary copolymer gel formulation of Perma-Gel™ relative to the model block copolymer gels, which alters the dynamic response of the network in a slightly different manner than simple diblock addition. Moreover, as the vol. %-diblock was increased in these styrenic materials, energy dissipation capacity increased.

From a materials design perspective, this increase in energy dissipation capacity within increasing vol. %-diblock can be rationalised by microstructural changes in the gel as a function of composition. As shown in Figure 2, these gels are comprised

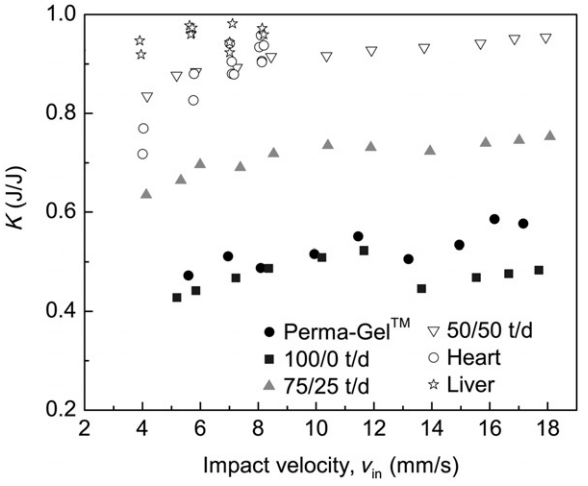

Figure 8. Energy dissipation parameter, K, as a function of impact velocity provides a quantitative comparison among samples. Whereas the tissues and 50/50 triblock/diblock gel dissipate nearly all of the imposed impact energy, Perma-Gel™ and 100/0 triblock/diblock gel dissipate only 40–50% of the total energy at these impact velocities.

of nm-scale micelles that include the styrenic segments of multiple di- or triblocks. Only triblocks have the capacity to bridge styrenic segments. Thus, decreasing the concentration of triblocks in the polymer will decrease the number of bridges formed between micelles. These bridges act as active chains in elastic energy restoration, as effective elastic springs [35]. Therefore, a decrease in the number of bridges will have a negative impact on the capacity of these gels to recover elastic strain energy. Finally, comparisons of Q among these materials showed that the 50/50 triblock/diblock ($Q = 1.68 \pm 0.05$) exhibited similar dissipation capacity rates as that measured for liver tissue ($Q = 1.77 \pm 0.07$).

To compare the high-rate response of each material quantitatively, the energetic dissipation parameter K (Equation (8)) was calculated as a function of impact velocity (Figure 8). In contrast to Q and v_{out}/v_{in}, K deconvolutes the finite damping of the impact pendulum from the impulse response of the sample. Liver tissue exhibited the highest magnitude of K, dissipating 95% of the impact energy at these impact energy densities; K_{liver} was independent of impact velocity. In contrast, K_{heart} was lower than that of liver and exhibited considerable velocity dependence. The tissue surrogate gels exhibited composition-dependent K, with $K_{50/50}$ well matched to that of heart tissue to dissipate ~90% of the total impact energy. Tissue surrogate gels exhibited either a weak, positive increase in K with impact velocity (75/25 and 50/50 triblock/diblock) or no discernible velocity dependence (100/0 triblock/diblock and Perma-Gel™). This contrast between the tissue types, as well as among the tissue surrogate gels, remains an area of open interpretation that may be related to poroelastic effects, micellar reconfiguration within gels, and/or lamellar structural heterogeneity of tissues. Although beyond the scope of the current study, the methods outlined herein can be implemented in future work to independently explore

the effects of penetration depth and contact volume on energy dissipation, e.g. through variation of the contact probe geometry for impact velocities of interest. Future applications of this method may also be designed to identify the possible additional contributions of nonlinear elastic deformation at these impact rates, provided that the macroscale stress–strain response of tissues or gels can be acquired to quantify any appreciable nonlinearity at the imposed strains and strain rates. Such implementations of the methods and analyses outlined here can enable multiscale analysis of energy dissipation in heterogeneous tissues, for distinct applications or models of scale-dependent deformation mechanisms.

At the high strain energy densities and velocities of primary interest for tissue surrogate applications, this quantitative analysis of energy dissipation and penetration depth of a given contact probe enables identification of promising tissue surrogate candidates. The 50/50 triblock/diblock styrenic gel is stable in air, and best replicates the extent of energy dissipation in the initial collision event that is exhibited by fully hydrated heart tissue (i.e. these materials exhibit K within 4% in Figure 8). Among the synthetic gels, this composition also exhibits penetration depths that are closest to those of heart tissue at all impact velocities (Figure 6a), though still exceeding the penetration resistance of heart tissue by at least $\sim$15%. This gel also best replicates the energy dissipation rate of these tissues, exhibiting Q within 23% and 5% of heart and liver tissues, respectively. Note that there exists a competition between energy dissipation capacity K and energy dissipation rate Q in these gels, as apparent from the fact that the 50/50 gel compares more closely to the energy dissipation capacity of heart tissue and to the energy dissipation rate of liver tissue. Together these findings indicate that Perma-Gel^{TM} and the 100/0 and 75/25 triblock/diblock styrenic gels are suboptimal surrogates for heart and liver tissues, in that these materials do not accurately predict impact loading resistance and impact energy dissipation capacity of these tissues. In contrast, the 50/50 triblock/diblock styrenic gel is a more suitable mechanical surrogate of heart and liver tissue, in terms of the rates and extents of energy dissipation. As noted, further optimisation of energy dissipation via this specific styrenic diblock/triblock gel is limited by the incomplete gelation for triblock composition <50 vol. %. However, the present experiments elucidate the role of crosslinking bridges among micelles as a strong determinant of impact energy dissipation, and will guide design of future block copolymers for these tissue surrogate applications.

4. Conclusions

The dynamic impact responses of styrenic triblock/diblock copolymer gels and a commercially available ballistic gel were studied and compared with those of fully hydrated liver and heart tissues. The specific tissue surrogate application of interest required comparable penetration resistance and impact energy dissipation capacity of these gels to that of liver and heart tissues. Neither commercial Perma-Gel^{TM} nor block copolymers of high vol. %-triblock accurately mimicked the responses of these tissues. However, observations of compositionally dependent energy dissipation capacity in the styrenic gels enabled development and demonstration of a 50/50 triblock/diblock gel that served as a strong surrogate of impact energy dissipation

capacity for these tissues. The instrumented dynamic impact indentation analyses detailed here thus enable further modifications of these and other tissue surrogate gels to quantitatively replicate the full energy dissipation response of hydrated soft tissues for a range of applications.

Acknowledgements

We thank Patrick Barragan for assistance with automation of the impact energy dissipation calculations via MATLAB. This research was supported in part by the US Army through the Institute for Soldier Nanotechnologies, under Contract W911NF-07-D-0004 with the US Army Research Office.

References

[1] T.F. Juliano, A.M. Foster, P.L. Drzal, T. Weesooriya, P. Moy and M.R. VanLandingham, J. Mater. Res. 21 (2006) p.2084.
[2] H. Saraf, K. Ramesh, A. Lennon, A. Merkle and J. Roberts, J. Biomech. 40 (2007) p.1960.
[3] M.L. Fackler and J.A. Malinowski, J. Trauma Inj. Infect. Crit. Care 25 (1985) p.522.
[4] Y.C. Fung, *Biomechanics: Mechanical Properties of Living Tissues*, Springer, New York, 1993.
[5] K. Miller, J. Biomech. 38 (2005) p.153.
[6] C. Chui, E. Kobayashi, X. Chen, I. Sakuma and T. Hisada, Med. Biol. Eng. Comput. 45 (2007) p.99.
[7] S.L. Barnes, A. Lyshchik, M.K. Washington, J.C. Gore and M.I. Miga, Med. Phys. 34 (2007) p.4439.
[8] D.M. Ebenstein and L.A. Pruitt, J. Biomed. Mater. Res. A 69 (2004) p.222.
[9] O. Franke, K. Durst, V. Maier, M. Goken, T. Birkholz, H. Schneider, F. Hennig and K. Gelse, Acta Biomater. 3 (2007) p.873.
[10] D.M. Ebenstein, A. Kuo, J.J. Rodrigo, A.H. Reddi, M. Ries and L. Pruitt, J. Mater. Res. 19 (2004) p.273.
[11] C. Li, L. Pruitt and K. King, J. Biomed. Mater. Res. A 78 (2006) p.729.
[12] D. Valtorta and E. Mazza, Med. Image Anal. 9 (2005) p.481.
[13] S. Park and G. Ateshian, J. Biomech. Eng. 128 (2006) p.623.
[14] D. Mavrillas, E. Sinouris, D. Vynios and N. Papageorgakopoulou, J. Biomech. 38 (2005) p.761.
[15] S. Nasseri, L.E. Bilston and N. Phan-Thien, Rheol. Acta 41 (2002) p.180.
[16] J.M. Matice, A.G. Lau, M.L. Oyen and R.W. Kent, J. Mater. Res. 21 (2006) p.2003.
[17] J. Snedker, M. Barbezat, P. Niederer, F. Scmidlin and M. Farshad, J. Biomech. 38 (2005) p.993.
[18] B. Song, W. Chen, Y. Ge and T. Weerasooriya, J. Biomech. 40 (2007) p.2999.
[19] C. Sligtenhorst, D. Cronin and G. Brodland, J. Biomech. 39 (2006) p.1852.
[20] H. Saraf, K. Ramesh, A. Lennon, A. Merkle and J. Roberts, Exp. Mech. 47 (2007) p.439.
[21] J.L. Lewis, L.B. Deloria, M. Oyen-Tiesma, R.C. Thompson, Jr., M. Ericson and T.R. Oegema, Jr., J. Orthop. Res. 21 (2003) p.881.
[22] F. Varga, M. Drzik, M. Handl, J. Chlpik, P. Kos, E. Filova, M. Rampichova, A. Necas, T. Trc and E. Amler, Physiol. Res. 56 (Suppl.1) (2007) p.S61.
[23] S.N. Robinovitch, T.A. McMahon and W.C. Hayes, J. Orthop. Res. 13 (1995) p.956.

[24] M. Balooch, I.-C. Wu-Magidi, A. Balazs, A.S. Lundkvist, S.J. Marshall, G.W. Marshall, W.J. Siekhaus and J.H. Kinney, J. Biomed. Mater. Res. 40 (1998) p.539.
[25] G. Constantinidies, C.A. Tweedie, D.M. Holbrook, P. Barragan, J.F. Smith and K.J. Van Vliet, Mater. Sci. Eng. A 489 (2008) p.403.
[26] G. Constantinides, C.A. Tweedie, N. Savva, J.F. Smith and K.J. Van Vliet, Exp. Mech. 49 (2009) p.511.
[27] MSDS Solutions (Doc. Ref. 2391940). Available at: http://www.msds.com/.
[28] R. Bowen, *Hepatic Histology: The Lobule*, 2003. Available at: http://www.vivo.colostate.edu/hbooks/pathphys/digestion/liver/histo_lobule.html.
[29] E.A. Ashley and J. Niebauer, *Cardiology Explained*, Remedica Medical Education and Publishing, 2005.
[30] J.R. Quintana, E. Hernaez and I. Katime, Polymer 43 (2002) p.3217.
[31] Y. Sliozberg, J. Andzelm, J.K. Brennan, M. Vanlandingham and V. Ganesan, J. Polym. Sci. B Polym. Phys. 48 (2010) p.15.
[32] G. Constantinides, I.Z. Kalcioglu, M. McFarland, J.F. Smith and K.J. Van Vliet, J. Biomech. 41 (2008) p.3285.
[33] A.P. French, *Vibrations and Waves*, W.W. Norton, New York, 1971.
[34] H.J. Pain, *The Physics of Vibrations and Waves*, John Wiley & Sons, England, 2005.
[35] J.H. Laurer, S.A. Khan, R.J. Spontak, M.M. Satkowski, J.T. Grothaus, S.D. Smith and J.S. Lin, Langmuir 15 (1999) p.7947.
[36] G.C. Engelmayr, Jr., M. Cheng, C.J. Bettinger, J.T. Borenstein, R. Langer and L.E. Freed, Nat. Mater. 7 (2008) p.1003.
[37] E. Roan and K. Vegemanti, J. Biomech. 129 (2007) p.450.